Report

Cell Reports

The Mitochondrial Calcium Uniporter Controls Skeletal Muscle Trophism In Vivo

Graphical Abstract

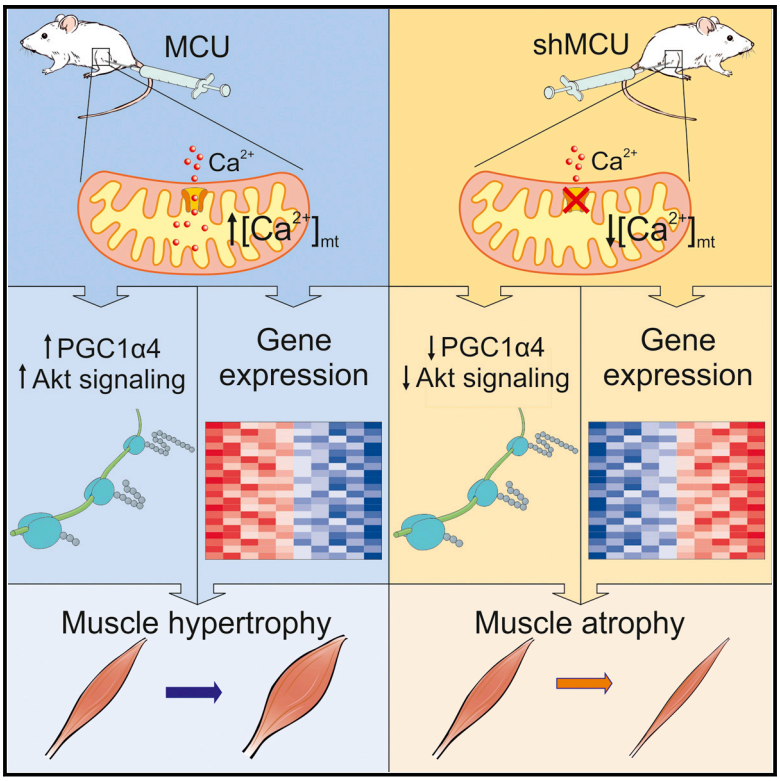

Highlights

- MCU controls mitochondrial Ca^{2+} uptake in skeletal muscle in vivo
- MCU is sufficient and required for muscle size control
- Mitochondria control hypertrophy signaling pathways
- MCU protects from denervation-induced atrophy

Authors

Cristina Mammucari, Gaia Gherardi, ..., Gerolamo Lanfranchi, Rosario Rizzuto

Correspondence

cristina.mammucari@unipd.it (C.M.), rosario.rizzuto@unipd.it (R.R.)

In Brief

Mammucari et al. show that mitochondrial Ca^{2+} uptake positively regulates skeletal muscle size in vivo. In particular, gain- and loss-of-function experiments demonstrate that modulation of the mitochondrial calcium uniporter (MCU) controls mitochondrial volume, hypertrophy signaling pathways, protein synthesis, and gene transcription. In addition, MCU overexpression counteracts denervation-induced atrophy.

Accession Numbers

GSE60931

Mammucari et al., 2015, Cell Reports *10*, 1269–1279
March 3, 2015
http://dx.doi.org/10.1016/j.celrep.2015.01.056

Cell Reports
Report

The Mitochondrial Calcium Uniporter Controls Skeletal Muscle Trophism In Vivo

Cristina Mammucari,[1,8,*] Gaia Gherardi,[1,8] Ilaria Zamparo,[1] Anna Raffaello,[1] Simona Boncompagni,[2] Francesco Chemello,[3] Stefano Cagnin,[3] Alessandra Braga,[1] Sofia Zanin,[1] Giorgia Pallafacchina,[1,4] Lorena Zentilin,[5] Marco Sandri,[1,4,6,7] Diego De Stefani,[1] Feliciano Protasi,[2] Gerolamo Lanfranchi,[3] and Rosario Rizzuto[1,4,*]
[1]Department of Biomedical Sciences, University of Padua, Padua 35131, Italy
[2]Ce.S.I. (Center for Research on Ageing) and D.N.I.C.S. (Department of Neuroscience, Imaging and Clinical Sciences), University "G. D'Annunzio" of Chieti, Chieti 66100, Italy
[3]Department of Biology and CRIBI Biotechnology Center, University of Padua, Padua 35131, Italy
[4]Neuroscience Institute, National Research Council, Padua 35131, Italy
[5]International Centre for Genetic Engineering and Biotechnology (ICGEB), Trieste 34159, Italy
[6]Dulbecco Telethon Institute at Venetian Institute of Molecular Medicine, Padua 35129, Italy
[7]Telethon Institute of Genetics and Medicine (TIGEM), Naples 80131, Italy
[8]Co-first author
*Correspondence: cristina.mammucari@unipd.it (C.M.), rosario.rizzuto@unipd.it (R.R.)
http://dx.doi.org/10.1016/j.celrep.2015.01.056

SUMMARY

Muscle atrophy contributes to the poor prognosis of many pathophysiological conditions, but pharmacological therapies are still limited. Muscle activity leads to major swings in mitochondrial [Ca^{2+}], which control aerobic metabolism, cell death, and survival pathways. We investigated in vivo the effects of mitochondrial Ca^{2+} homeostasis in skeletal muscle function and trophism by overexpressing or silencing the mitochondrial calcium uniporter (MCU). The results demonstrate that in both developing and adult muscles, MCU-dependent mitochondrial Ca^{2+} uptake has a marked trophic effect that does not depend on aerobic control but impinges on two major hypertrophic pathways of skeletal muscle, PGC-1α4 and IGF1-Akt/PKB. In addition, MCU overexpression protects from denervation-induced atrophy. These data reveal a novel Ca^{2+}-dependent organelle-to-nucleus signaling route that links mitochondrial function to the control of muscle mass and may represent a possible pharmacological target in conditions of muscle loss.

INTRODUCTION

Loss of muscle mass and performance, together with important metabolic changes, occurs in pathophysiological conditions such as aging (sarcopenia), disuse, denervation, starvation, and cancer (cachexia). Therapeutic interventions aimed at preserving muscle mass are of key importance, but they are still limited. Skeletal muscle size is determined by the equilibrium between protein synthesis and degradation, which in turn is controlled by different signaling. In particular, the insulin-like growth factor 1-Akt/protein kinase B (IGF1-Akt/PKB) pathway controls muscle size by impinging both on protein translation via mammalian target of rapamycin (mTOR) and glycogen synthase kinase 3β (GSK3β) and on protein degradation via the ubiquitin-proteasome and autophagy-lysosome pathways (Mammucari et al., 2008). In addition, a novel isoform of the mitochondria-related PGC-1α family of transcription coactivators, namely PGC-1α4, has been recently shown to trigger muscle hypertrophy (Ruas et al., 2012).

Mitochondria play a central role in skeletal muscle function by providing ATP largely consumed by SERCA activity and actomyosin contraction. The tight coupling of mitochondrial ATP production to the requirements of a contracting muscle is ensured by effects of the ubiquitous second messenger Ca^{2+} on aerobic metabolism. In a wide variety of cell types, including primary cultures of skeletal myotubes (Brini et al., 1997) and muscle fibers in situ (Rudolf et al., 2004), cytosolic Ca^{2+} transients generated by physiological stimuli elicit large increases in the [Ca^{2+}] of the mitochondrial matrix ($[Ca^{2+}]_{mt}$), which in turn stimulate the Ca^{2+}-sensitive dehydrogenases of the Krebs cycle. At the same time, $[Ca^{2+}]_{mt}$ rises have been shown to inhibit autophagy (Cárdenas et al., 2010) and sensitize cells to apoptosis and necrotic challenges (for review, see Rizzuto et al., 2012).

The recent identification of the mitochondrial calcium uniporter (MCU) (Baughman et al., 2011; De Stefani et al., 2011), the highly selective channel responsible for Ca^{2+} entry into mitochondria, allows us to investigate in detail its role in different aspects of skeletal muscle biology. Genetic ablation of MCU in the germline, however, displayed a mild phenotype (Pan et al., 2013). A clear indication of the importance of MCU-dependent mitochondrial Ca^{2+} accumulation in skeletal muscle function was the recent identification of a mutation of MICU1, a direct modulator of MCU, in patients with proximal muscle weakness, learning difficulties, and extrapyramidal motor disorder (Logan et al., 2014).

In this report, we investigated the role of MCU in skeletal muscle by overexpressing or silencing MCU after birth in order to rule out compensatory effects during prenatal development. The

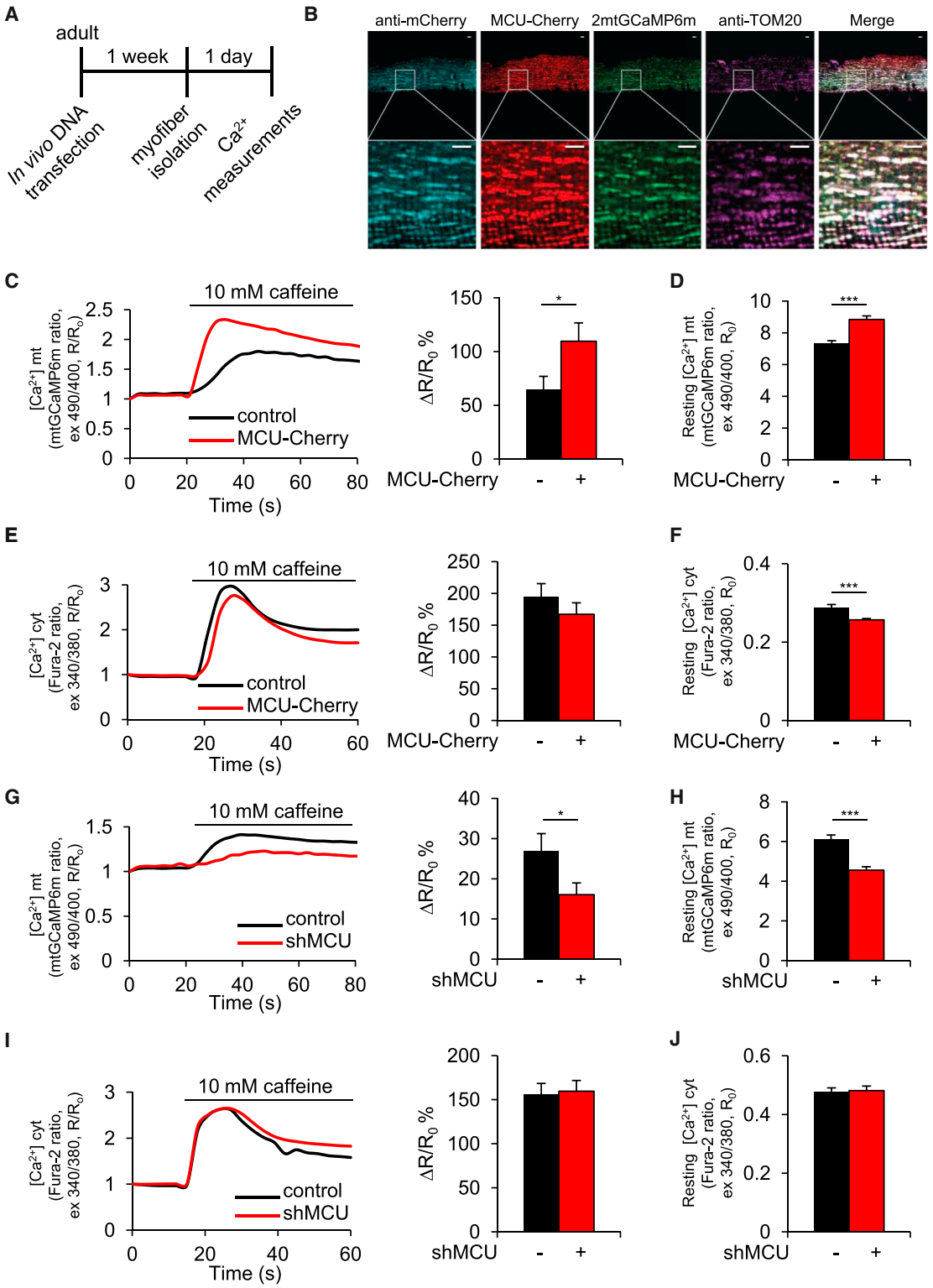

Figure 1. MCU Is Sufficient and Required for Mitochondrial Ca^{2+} Uptake in Skeletal Muscle Ex Vivo

(A) Flexor digitorum brevis (FDB) muscles were transfected with mtGCaMP6 and MCU-Cherry or shMCU. pmCherry-N1 or shluc was used as a control, respectively. Seven days later, single myofibers were isolated and placed in culture.

(B) Immunofluorescence analysis shows colocalization of MCU-Cherry and mtGCaMP6 with the mitochondrial protein TOM20 in muscle fibers processed as in (A). Scale bar, 5 μm.

(legend continued on next page)

results show that MCU expression triggers hypertrophy, both during post-natal growth and in adulthood, by controlling protein synthesis through the PGC-1α4 and IGF1-Akt/PKB pathways. Finally, MCU exerts a protective effect against atrophy, suggesting that modulation of mitochondrial Ca^{2+} uptake may represent a novel area of therapeutic intervention to combat muscle mass loss.

RESULTS

MCU Overexpression or Silencing In Vivo Affects Mitochondrial Ca^{2+} Uptake in Muscle Fibers

In cultured cells, modulation of MCU expression determines the amplitude of mitochondrial Ca^{2+} uptake upon physiological stimuli (De Stefani et al., 2011). In this work, we decided to specifically alter mitochondrial Ca^{2+} uptake in vivo by adeno-associated virus (AAV) serotype 9-based transduction or muscle transfection with MCU plasmids. To verify the efficacy of this approach, we transfected adult flexor digitorum brevis (FDB) mouse muscles in vivo with plasmids encoding a GFP-based Ca^{2+} probe targeted to mitochondria, mtGCaMP6m (Logan et al., 2014), in combination with a plasmid encoding mCherry (control) or mCherry-tagged MCU (MCU-Cherry). Eight days later, real-time imaging experiments were performed on isolated single myofibers (Figure 1A). Both MCU-Cherry and mtGCaMP6m colocalize with the mitochondrial protein TOM20 in muscle fibers (Figure 1B). After assessment of basal Ca^{2+} concentrations, a cytosolic and hence mitochondrial $[Ca^{2+}]$ rise was evoked by discharging the sarcoplasmic reticulum (SR) pool with caffeine. MCU overexpression caused a marked increase in the caffeine peak and a modest elevation of the resting $[Ca^{2+}]_{mt}$ (Figures 1C and 1D). Cytosolic Ca^{2+} levels were almost unaffected by MCU, showing a small decrease that was statistically significant for resting values (Figures 1E and 1F). The silencing experiments gave coherent results. FDB muscles were co-transfected in vivo with plasmids encoding either shluc (control) or shMCU and mtGCaMP6m. Ex vivo imaging experiments showed a marked reduction of both $[Ca^{2+}]_{mt}$ resting values and caffeine-induced peaks in shMCU-transfected fibers (Figures 1G and 1H), while cytosolic Ca^{2+} values were virtually unaffected (Figures 1I and 1J). In order to mimic the physiological response of innervated muscles, we also measured Ca^{2+} transients upon K^+-induced depolarization. Similarly to the caffeine experiments, higher and lower $[Ca^{2+}]_{mt}$ peaks were detected in MCU overexpression and silencing, respectively, although Ca^{2+} transients were smaller and shorter than caffeine-evoked transients. Interestingly, the opposite effect was detected in the $[Ca^{2+}]_{cyt}$ peak, indicating a role of mitochondria as cytosolic Ca^{2+} buffers in vivo (Figures S1A–S1D). Importantly, neither MCU nor shMCU affected $\Delta\psi$ (Figures S1E and S1F), thus ruling out an indirect effect on the driving force for mitochondrial Ca^{2+} accumulation.

MCU Controls Muscle Size during Post-natal Growth

We thus investigated the role of MCU in both developing and adult muscle. We first focused on developing muscle, in which a greater plasticity could be expected. We injected hindlimb muscles of newborn mice with AAV-MCU and analyzed the muscles eight weeks later (Figure 2A). A striking phenotype affecting muscle trophism was observed. MCU overexpression, confirmed by western blotting of cytosolic and mitochondrial fractions (Figure 2B) and by immunofluorescence (Figure 2C), resulted in 47% increase in the average fiber area of MCU-infected tibialis anterior (TA) compared to controls (Figure 2D). When measured 1 month after injection, TA muscle fiber size was 28% greater than control fibers (Figure S2), indicating a progressive event that starts early after injection and continues up to 2 months of age. To verify whether MCU-induced hypertrophy affected also different fiber types, we investigated soleus muscles, which are mitochondria-rich slow muscles. MCU triggered 41% hypertrophy compared to controls, suggesting that the effect of mitochondrial Ca^{2+} uptake in hypertrophy is independent of the number of mitochondria and of the overall metabolic properties (Figure 2E). Next, we analyzed the effect of MCU silencing. Newborn hindlimb muscles were injected with AAV-shMCU and fiber size measured 2 months later. AAV-shMCU was efficiently delivered to TA muscle (Figure 2F) and decreased MCU protein expression (Figure 2G). Fiber size was markedly reduced both in TA and in soleus muscles (−30% and −28%, respectively) (Figures 2H and 2I), highlighting the requirement of mitochondrial Ca^{2+} signals for the maintenance of skeletal muscle trophism.

Mitochondrial Structure and Function in MCU Overexpression and Silencing

We then investigated the cellular changes that could underlie the trophic effect of MCU. We first focused on the effect on mitochondrial morphology and volume by electron microscopy (EM) and on their metabolic properties. In extensor digitorum longus (EDL) fibers from adult control mice, mitochondria are positioned almost exclusively at the I band on both sides of the Z-lines (Boncompagni et al., 2009) (Figure 3A, arrows); in longitudinal sections, their profiles appear round or oval, with parallel cristae within a dark/electron dense matrix (Figure 3B). In MCU-overexpressing EDL fibers, although many mitochondria

(C) Left: representative traces of mitochondrial Ca^{2+} dynamics in a pmCherry-N1 (control, black trace) or MCU-Cherry (red trace) expressing fiber upon caffeine stimulation. Right: mean mitochondrial $[Ca^{2+}]$ increase. n = 25.
(D) Resting mitochondrial $[Ca^{2+}]$. n = 60.
(E) Left: representative traces of cytosolic Ca^{2+} dynamics. Right: mean cytosolic $[Ca^{2+}]$ increase. n = 18.
(F) Resting cytosolic $[Ca^{2+}]$. n = 25.
(G) Left: representative traces of mitochondrial Ca^{2+} dynamics in an shluc-Cherry-expressing (control, black trace) or shMCU-Cherry-expressing (shMCU, red trace) fiber. Right: mean mitochondrial $[Ca^{2+}]$ increase. n = 36.
(H) Resting mitochondrial $[Ca^{2+}]$. n = 36.
(I) Left: representative traces of cytosolic Ca^{2+} dynamics. Right: mean cytosolic $[Ca^{2+}]$ increase. n = 23.
(J) Resting cytosolic $[Ca^{2+}]$. n = 23. In each panel, data are presented as mean ± SEM. *$p < 0.05$, ***$p < 0.001$, t test (two-tailed, unpaired).
See also Figure S1.

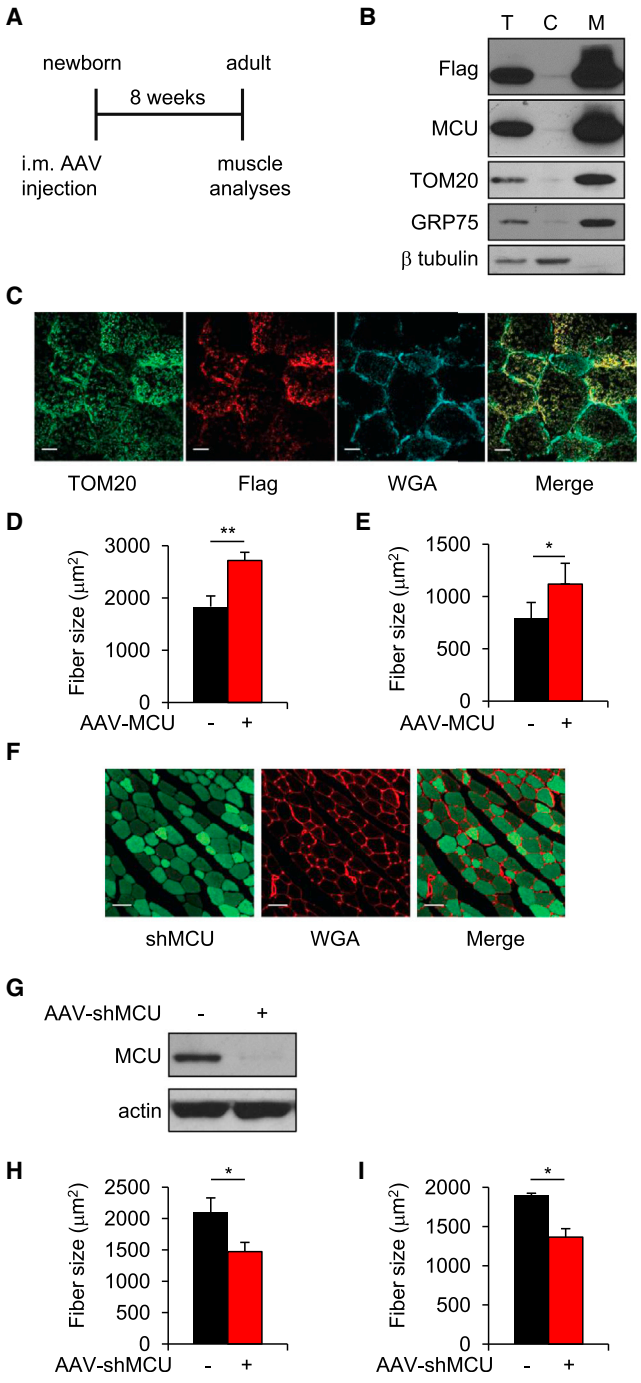

Figure 2. MCU Controls Muscle Size during Post-natal Growth

(A) Hindlimb muscles of newborn mice (4–6 days old) were injected with Flag-tagged AAV-MCU or AAV-shMCU. AAV-LacZ and AAV-shluc were used as negative controls, respectively. Two months later, muscles were isolated and processed for further analysis.

(B) Immunoblotting of total protein lysates (T) and cytosolic (C) and mitochondrial (M) fractions of TA muscles infected with AAV-MCU. Anti-Flag antibody was used to detect AAV-MCU. TOM20 was used as marker of outer mitochondrial membrane, GRP75 for the mitochondrial matrix, and β tubulin for the cytosol.

appeared normal in shape and correctly localized with respect to the sarcomere (Figure 3C, arrows), we found some atypical mitochondria, which form wavy stacks of cristae protruding as long tentacles in inter-myofibrillar spaces (Figure 3C, arrowheads, and enlargements in Figures 3D–3F). These mitochondria, considered abnormal mitochondria in the quantitative analysis (Figure 3I, column e), accounted for <10% of all mitochondria. Further quantitative investigation revealed that the fiber volume occupied by mitochondria increased from ~3.5% to ~4.5% (Figure 3I, column a), possibly due to the increase in the average mitochondrial diameter (Figure 3I, column c). In MCU-silenced fibers, the atypical wavy mitochondria observed in MCU-overexpressing fibers were never detected. In addition, the relative fiber volume occupied by mitochondria was significantly reduced, in parallel with a decreased number and size of these organelles (Figure 3G, arrows and 3I, columns a–c). The frequency of severely damaged mitochondria, i.e., presenting vacuoles and disrupted cristae (Figure 3G, arrowheads) or containing myelin figures (Figure 3H) and longitudinally oriented organelles (Figure 3G, star), was also increased (6.1% versus 1.5% of controls) (Figure 3I, columns d and e).

Next, we investigated the effects on mitochondrial aerobic metabolism, focusing on the Ca^{2+}-regulated enzymatic steps, such as pyruvate dehydrogenase (PDH). MCU overexpression affected neither the phosphorylation levels of PDH (Figure S3A) nor PDH activity (Figure 3J). A qualitative histochemical analysis of the activity of SDH, COX IV, and NADH-TR in TA muscles did not show significant differences between MCU-overexpressing and control muscles. In addition, no difference was observed in glycogen content, as shown by PAS staining (Figure S3C). A comparative analysis of glycolytic (EDL) versus oxidative (soleus) muscles further confirmed that MCU overexpression does not qualitatively alter PAS and SDH activity (Figure S3D). Similar analyses were conducted on AAV-shMCU-infected muscles. In agreement with data on MCU-depleted muscles (Pan et al., 2013), MCU silencing increased PDH phosphorylation (Figure S3B) and decreased PDH activity (Figure 3K), although no significant changes in the histochemical pattern of SDH, COX IV, and NADH-TR were observed (Figure S3E). The amount of glycogen was also unaffected (Figure S3E). Overall, significant differences in mitochondrial volume were detected, but no obvious changes in structure and metabolic activity were observed that could be directly correlated with an effect on muscle size.

(C) TA muscle cryosections were immunostained with anti-TOM20 and anti-Flag antibodies. Wheat germ agglutinin (WGA) was used to label the sarcolemma. Scale bar, 20 μm.

(D) Mean fiber size of TA muscles. More than 600 fibers were measured for each muscle. n = 3.

(E) Mean fiber size of soleus muscles (>400 fibers per muscle; n = 3).

(F) Cryosection of AAV-shMCU infected TA muscle. shMCU was detected by ZsGreen fluorescence. Scale bar, 50 μm.

(G) Immunoblotting of TA muscles infected with AAV-shMCU.

(H) Mean fiber size of TA muscles (>600 fibers per muscle; n = 3).

(I) Mean fiber size of soleus muscles (>500 fibers per muscle; n = 3). In each panel, data are presented as mean ± SEM. *p < 0.05, **p < 0.01, t test (two-tailed, paired).

See also Figure S2.

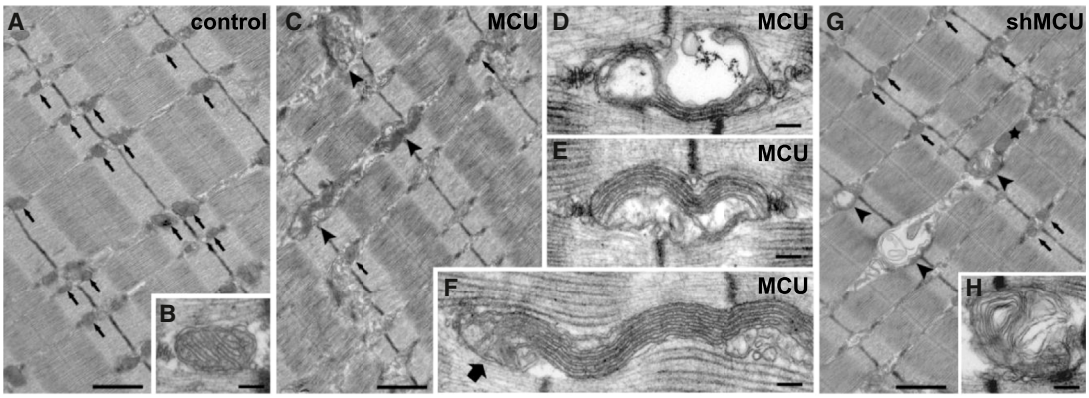

I

	a	b	c	d	e
	mt V/ total V, %	number of mt/ 100 μm²	average mt diameter, nm	number of mt at A band/ 100 μm²	% of severely damaged mt
control	3.5 ± 1.7	35 ± 12	210 ± 60 (592)	0.5 ± 1.2	2.6 (2777)
MCU	4.5 ± 1.5**	32 ± 7	235 ± 84 (445)**	1.1 ± 1.6**	5.6 (1449)**
shluc	3.3 ± 1.7	34 ± 12	212 ± 53 (267)	0.9 ± 1.5	1.5 (2692)
shMCU	2.5 ± 1.4**	27 ± 9**	182 ± 72 (316)**	1.8 ± 1.9**	6.1 (1866)**

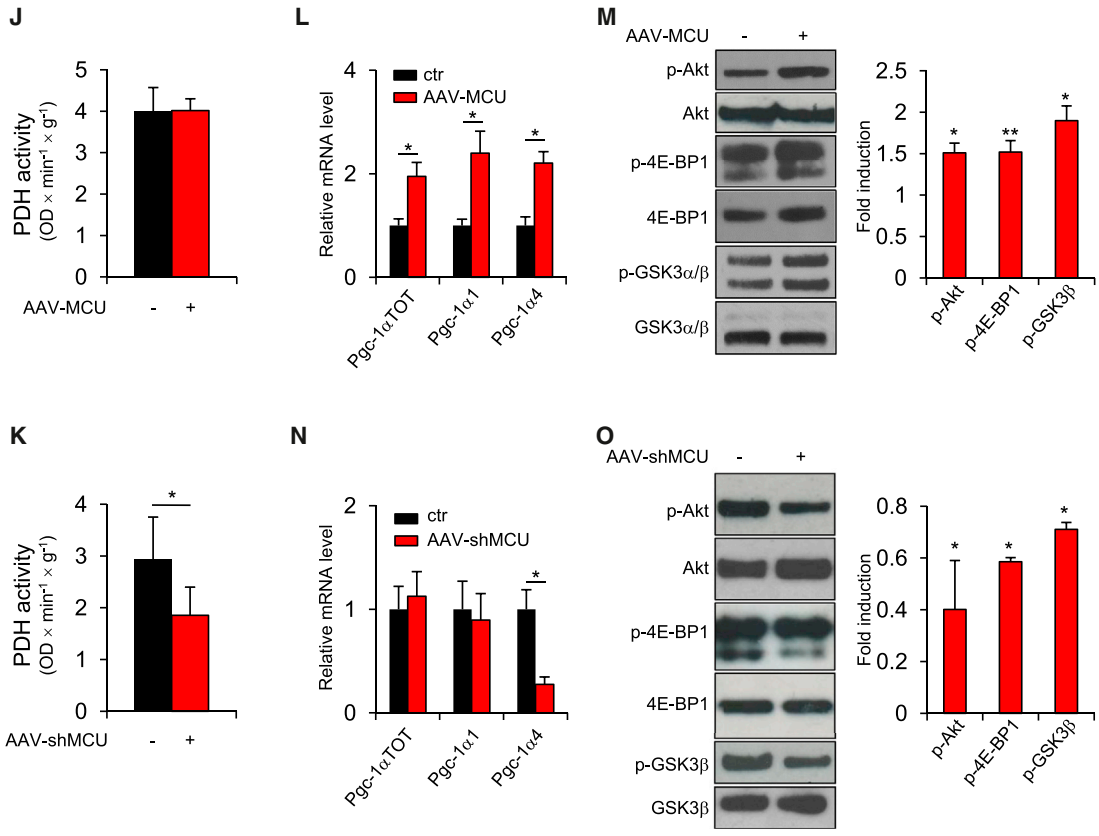

Figure 3. Effects of MCU Modulation on Mitochondrial Structure and Function and on Hypertrophy-Related Pathways during Muscle Development

(A–H) EM analysis of EDL muscles. Scale bars represent 1 μm (A, C, and G) or 0.1 μm (B, D–F, and H).

(I) Quantitative EM analysis. Values in columns a–d are shown as mean ± SD. In brackets is the total number of mitochondrial profiles evaluated in the analysis. **p < 0.01, t test (two tailed, paired) of three muscles per group.

(legend continued on next page)

MCU Regulates Muscle Hypertrophy Signaling Pathways

Since preliminary analysis showed no difference in autophagy (data not shown; Figure S3F), we focused our attention on the well-established hypertrophy pathways of skeletal muscle, PGC-1α4 and the IGF1-Akt/PKB axis. PGC-1α is the master regulator of mitochondriogenesis, and a novel PGC-1α isoform (PGC-1α4) has been reported to trigger muscle hypertrophy (Ruas et al., 2012). Analysis of the mRNA expression of the *Pgc-1α* isoforms demonstrated that AAV-MCU triggers induction of both *Pgc-1α1* and *Pgc-1α4* (Figure 3L), thus revealing both an enhanced mitochondriogenesis (in agreement with the ultrastructural analysis) and a stimulation of the PGC-1α-related hypertrophy pathway. Activation of IGF1-Akt/PKB triggers hypertrophy, while its suppression determines muscle atrophy (Schiaffino and Mammucari, 2011). In addition, IGF1-Akt/PKB signaling is activated by PGC-1α4 (Ruas et al., 2012). Accordingly, Akt was phosphorylated, and thus activated, by AAV-MCU (Figure 3M). Specific Akt downstream targets were phosphorylated: in detail, 4E-BP1 and GSK3β, two inhibitors of protein translation (Schiaffino and Mammucari, 2011), were phosphorylated, and thus inhibited, in AAV-MCU muscles (Figure 3M). These data suggest that MCU-mediated hypertrophy is due to increased PGC-1α4 and IGF1-Akt/PKB-dependent signaling. Finally, satellite cells also contribute to normal muscle growth. Analysis of Pax7-positive nuclei demonstrated that MCU caused an increase in the average satellite cells number per fiber (Figure S3G).

Next, we checked whether the same hypertrophy pathways were also suppressed by MCU silencing. *Pgc-1α4* expression was decreased by AAV-shMCU, while *Pgc-1α1* was unaffected (Figure 3N). In addition, the Akt signaling pathway was inactivated by shMCU, as demonstrated by decreased phosphorylation of Akt, 4E-BP1, and GSK3β (Figure 3O). Finally, satellite cell number was decreased in shMCU-infected muscles (Figure S3H). Overall, the above data indicate that MCU-mediated mitochondrial Ca^{2+} homeostasis regulates skeletal muscle size during post-natal growth by directly impinging on specific master regulators of hypertrophy.

MCU Acutely Controls Muscle Size in the Adult

We proceeded to the analysis of adult muscle, where an effect on muscle trophism could have direct relevance for the understanding and potential targeting of age- and disease-related loss of muscle mass. For this purpose, adult EDL muscles were infected with AAV-MCU or AAV-shMCU, and fiber size was measured 2 weeks later (Figure 4A). AAV-MCU infection triggered a 37% increase in fiber size (Figure 4B) while AAV-shMCU infection caused a 31% decrease, thus demonstrating that mitochondrial Ca^{2+} uptake is required for muscle trophism also in the adult (Figure 4C).

Adult muscle size is regulated by a fine equilibrium between protein synthesis and protein degradation of myofibrillar components. We analyzed protein synthesis by ''surface sensing of translation'' (SUnSET), a method based on the incorporation of puromycin into nascent peptide chains that allows accurate detection of protein synthesis rate in skeletal muscle in vivo (Goodman et al., 2011). Puromycin was injected to adult mice infected with AAV-MCU, and muscles were analyzed 30 min later. Detection of puromycin with specific antibodies showed that protein synthesis was strongly induced by MCU (Figure 4D). As in developing muscle, the experiments in adult muscle also revealed a marked effect of MCU on PGC-1α4 and the IGF1-Akt/PKB axis. In particular, *Pgc-1α4* was drastically upregulated upon MCU overexpression and downregulated upon MCU silencing (Figures 4E and 4F). In contrast to post-natal muscles, the effects on total *Pgc1-α* and *Pgc1-α1* levels were very modest and did not correlate with the *Pgc1-α4* change, thus suggesting a specific effect on the PGC1-α4-related hypertrophy pathway. Similarly, analysis of the IGF1-Akt/PKB trophic pathway provided a coherent picture, with phosphorylation of Akt and downstream targets in MCU-overexpressing muscles (Figure 4G) and the opposite effect upon MCU silencing (Figure 4H). Finally, the number of Pax7-positive cells was unaffected by MCU, suggesting a marginal role of the satellite cell compartment in MCU-induced muscle hypertrophy in the adult (Figures S4A and S4B).

Finally, to get a broader view of the MCU-dependent transcriptional changes and the pathways involved in the trophic effect, we carried out RNA microarray analyses of single myofibers of AAV-MCU- and AAV-shMCU-infected muscles, with respective controls.

Cluster analysis, according to the self-organizing tree algorithm (SOTA) (Herrero et al., 2001), revealed that AAV infection per se affected most differentially expressed genes (clusters 1, 5, 6, 8, 9, and 10) (Figure 4I). However, these genes do not play a role in muscle trophism, since infection with control AAV did not affect muscle size (data not shown). The remaining clusters included genes induced by MCU overexpression (clusters 2, 3, and 4) or silencing (clusters 7 and 11). Interestingly, genes activated 14 days after AAV-MCU infection (clusters 2 and 4) were enriched for components of the cytoskeleton or genes involved in sarcomere organization and Ca^{2+} homeostasis (Table S1). Genes in clusters 2 and 4 were activated by AAV-MCU infection and inhibited by MCU silencing (Figure S4C). A gene set enrichment analysis (GSEA) revealed that several pathways involved in hypertrophy were activated by MCU overexpression, including the insulin and mTOR signaling pathways (Table S2). It is interesting to note that most activated genes in response to MCU

(J) PDH activity of AAV-MCU infected TA muscles. n = 4.
(K) PDH activity of AAV-shMCU infected TA muscles. n = 10.
(L) Real-time RT-PCR analyses of AAV-MCU infected TA muscles. n = 4.
(M) Left: immunoblotting of AAV-MCU infected TA muscles. Right: quantification by densitometry. n = 4.
(N) Real-time RT-PCR analyses of AAV-shMCU TA infected muscles. n = 4.
(O) Left: immunoblotting of AAV-shMCU infected TA muscles. Right: quantification. n = 4. In (J)–(O), data are presented as mean ± SEM. *$p < 0.05$, **$p < 0.01$, t test (two tailed, paired).
See also Figure S3.

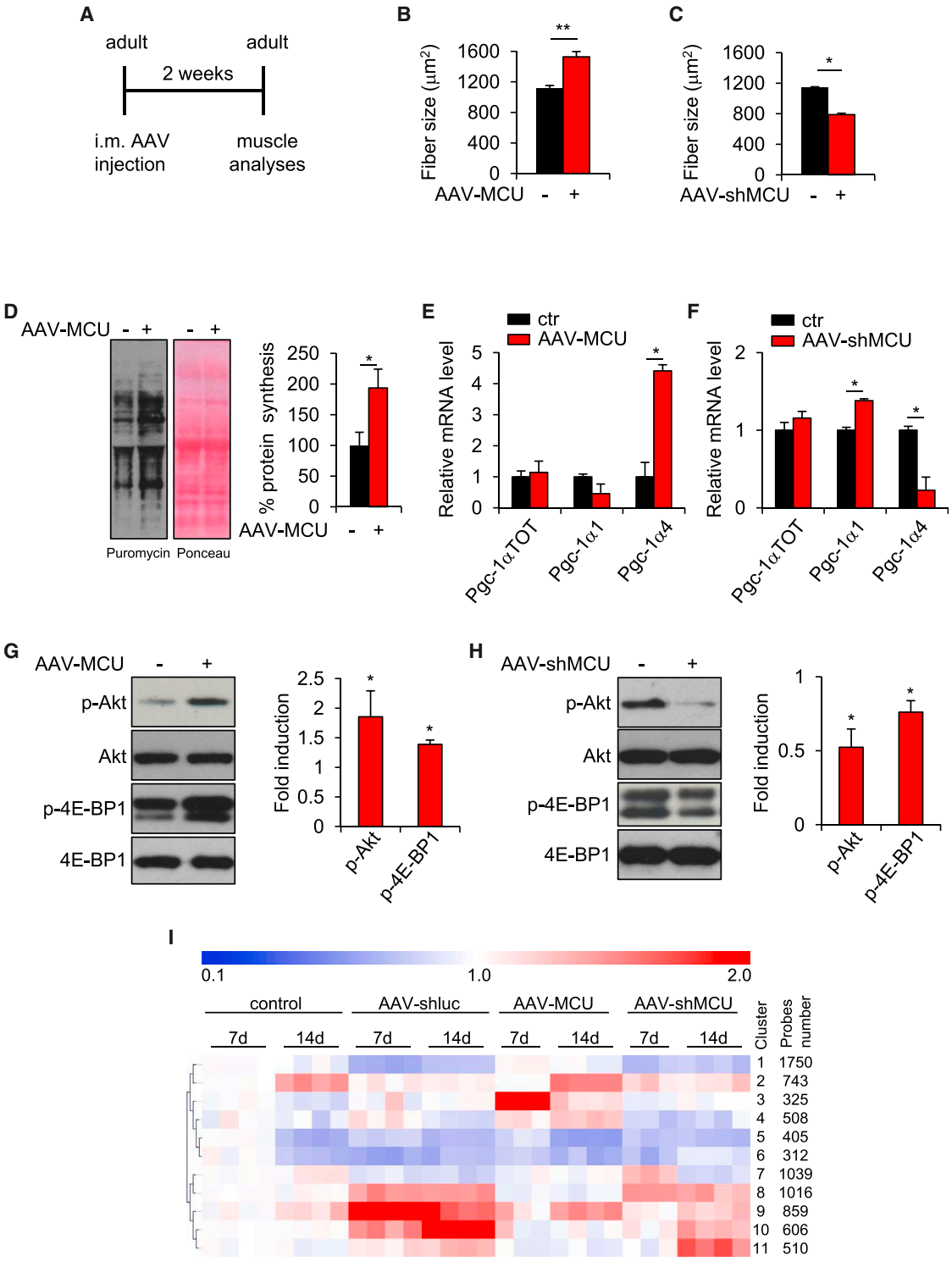

Figure 4. MCU Acutely Controls Muscle Size in the Adult

(A) EDL muscles of adult mice (2–3 months old) were infected with AAV-MCU or AAV-shMCU. AAV-LacZ or AAV-shluc was used as a negative control, respectively. Two weeks later, muscles were isolated and processed for further analysis.

(B and C) Mean fiber size of AAV-MCU- and AAV-shMCU-infected muscles (> 300 fibers per muscle; n = 3).

(D) Protein synthesis analysis. EDL muscles were infected with AAV-MCU for 2 weeks. Puromycin was then intraperitoneally injected, and muscles were isolated 30 min later. Left: western blotting with anti-puromycin antibodies. Ponceau S staining was used as loading control. Right: quantification. n = 4.

(legend continued on next page)

silencing (clusters 7 and 11) have mitochondrial functions (Table S3).

MCU Protects from Skeletal Muscle Atrophy

Finally, we investigated whether MCU overexpression could counteract conditions of disease-induced loss of muscle trophism. Denervation atrophy was triggered by sciatic nerve section, and Ca^{2+} signaling properties, together with muscle size, were evaluated (Figure 5A). Upon denervation, the cytosolic Ca^{2+} increase evoked by caffeine-induced SR release was markedly larger, although it did not evoke a larger Ca^{2+} uptake by mitochondria (Figures 5B and 5D), possibly due to the morphological remodeling of the fiber or alterations in the MCU complex assembly or SR/mitochondria coupling. Mitochondrial $\Delta\psi$ was unchanged (Figure S5A). However, when MCU was overexpressed, mitochondrial Ca^{2+} uptake, induced by caffeine-evoked SR release, was greatly enhanced, reaching peak values that, due to the robust cytosolic rise, exceeded those of non-denervated fibers (Figures 5B and 5D). As to resting values, a significant difference (i.e., a higher $[Ca^{2+}]_{mt}$ and lower $[Ca^{2+}]_{cyt}$ resting value) was detected only in MCU-expressing non-denervated muscle, while denervated muscles exhibited a value similar to controls, irrespective of MCU expression (Figures 5C and 5E). The measurements of $[Ca^{2+}]_{mt}$ and $[Ca^{2+}]_{cyt}$ transients upon K^+-induced depolarization gave similar results (Figures S5B and S5C).

We then evaluated muscle size. Denervation caused a 40% reduction in TA mean fiber size, as expected. When MCU was overexpressed, atrophy was reduced to ~16% compared to innervated control fibers (Figures 5F and 5G). Similar results were obtained when denervation was induced in adult animals in which MCU overexpression was induced by perinatal AAV infection (i.e., the conditions of Figures 2 and 3). In this case, fiber size was measured 3, 7, and 14 days post-denervation (Figures 5H and 5I). In control muscles, 17%, 30%, and 50% atrophy was observed, respectively, while in AAV-MCU-infected muscles, only 6%, 11%, and 22% reduction in fiber area was measured, respectively. Overall, the above data indicate that MCU overexpression can strongly counteract pathological atrophy.

DISCUSSION

The recent molecular identification of MCU (Baughman et al., 2011; De Stefani et al., 2011), and of its complex regulatory system (De Stefani and Rizzuto, 2014), now allows us to molecularly validate the broad literature supporting the pleiotropic role of mitochondrial Ca^{2+} homeostasis in cell function and survival. MCU-dependent mitochondrial Ca^{2+} accumulation was shown to play a role in pancreatic β cells (Alam et al., 2012; Tarasov et al., 2012), heart (Drago et al., 2012; Joiner et al., 2012), neurons (Qiu et al., 2013), and colon cancer (Marchi et al., 2013). In this scenario, the very mild phenotype of the $Mcu^{-/-}$ mouse was quite surprising (Pan et al., 2013). The observation that viable mice could be obtained only in a mixed genetic background, while MCU ablation was embryonically lethal in the inbred stains, points to yet-unresolved compensatory mechanisms (Murphy et al., 2014). Interestingly, the $Mcu^{-/-}$ mice show clear metabolic and functional alterations of skeletal muscle, and a MICU1 mutation (with ensuing loss of MCU gatekeeping, and hence increase in resting $[Ca^{2+}]_{mt}$ levels) was identified in subjects with a pathology comprising learning difficulties and early-onset proximal muscle weakness (Logan et al., 2014).

In our work, we bypassed embryonic development by utilizing viral transduction and in vivo electroporation for directing an MCU expression system or MCU small hairpin RNAs to the muscle of living animals. Two stages (developing and adult skeletal muscle) that exhibit intrinsic differences in plasticity and signaling responses were independently assessed, and a clear coherent phenotype was apparent, with some differences that are worthy of attention. Indeed, in both cases, mitochondrial Ca^{2+} accumulation via MCU positively correlated with the size of muscle fibers, i.e., a marked increase and reduction was observed in MCU-overexpressing and MCU-silenced fibers, respectively. In developing muscle, an increase in satellite cells was observed in MCU overexpressers (and a reduction in MCU-silenced fibers), but this was not the case in adult muscle, possibly due to the quiescent state of satellite cells in the adult. This result indicates that an effect on the stem cell reservoir of muscle is not the key mechanism underlying the MCU-dependent increase in muscle mass.

We thus explored two different potential mechanisms for the increase in fiber size: a purely metabolic effect and a regulation of the anabolic/catabolic balance of skeletal muscle. The first mechanism was unlikely for the following reasons: (1) PDH activity, albeit defective in MCU-silenced muscles (as in the $Mcu^{-/-}$ mouse), was unaffected by MCU overexpression; (2) the hypertrophic response was very similar in oxidative and glycolytic muscles, where the effect on mitochondrial metabolism should play a relatively minor role; and (3) semiquantitative analyses of aerobic metabolism revealed no major alteration. Nonetheless, electron microscopy (EM) analyses of MCU-silenced fibers showed an overall reduction in mitochondrial volume (and some mitochondrial damage), while MCU-overexpressing fibers showed increased mitochondrial volume and a peculiar proliferation of cristae, thus suggesting a role of mitochondrial Ca^{2+} homeostasis in the regulation of organelle biogenesis and morphology.

As to the anabolic/catabolic balance, we saw no difference in vivo in the autophagic rate, which we expected could be involved based on the induction of AMPK-dependent autophagy by inhibition of mitochondrial Ca^{2+} uptake (Cárdenas et al.,

(E and F) Real-time RT-PCR analyses of AAV-MCU- and AAV-shMCU-infected muscles. n = 4.
(G and H) Left: immunoblotting of AAV-MCU and AAV-shMCU infected muscles. Right: quantification. n = 4.
(I) Expression pattern clustering according to the self-organizing tree algorithm (SOTA). Gene expression values are relative to the average expression in control condition (7 days).
In (B)–(H), data are presented as mean ± SEM. *$p < 0.05$, **$p < 0.01$, t test (two tailed, paired).
See also Figure S4 and Tables S1, S2, and S3.

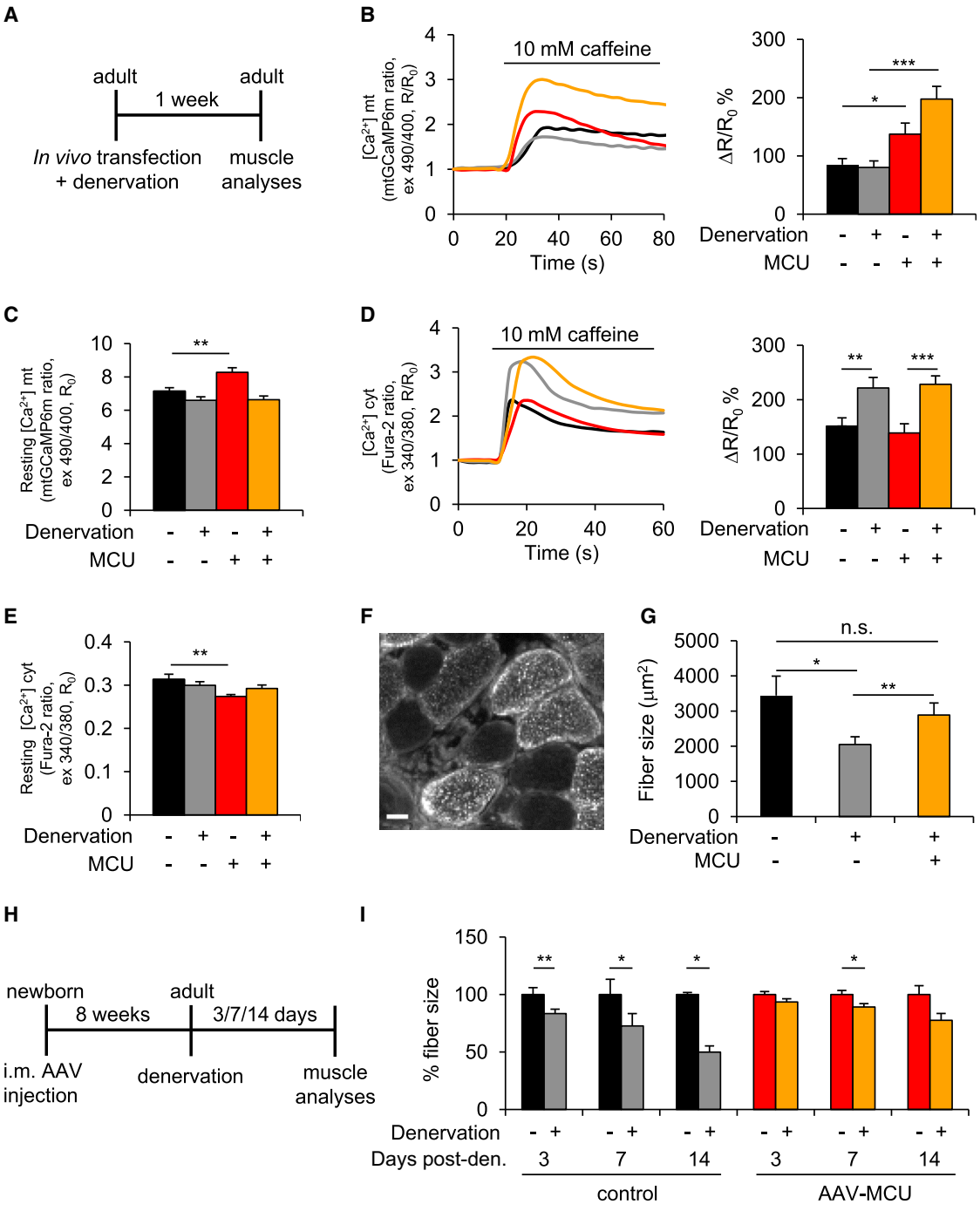

Figure 5. MCU Protects from Skeletal Muscle Atrophy

(A) Adult mice muscles were transfected with plasmids encoding MCU-Cherry (for real-time imaging) or MCU-Flag (for fiber-size analysis). At the same time, denervation was achieved by cutting the sciatic nerve high in the thigh. One week later, muscles were isolated and processed for further analysis.

(B) Mitochondrial Ca^{2+} uptake of denervated FDB muscles transfected with mCherry-N1 or MCU-Cherry (MCU) upon caffeine stimulation. Left: representative traces. Right: mean mitochondrial [Ca^{2+}] increase. n = 31.

(C) Resting mitochondrial [Ca^{2+}]. n = 51.

(D) Cytosolic Ca^{2+} transients. Left: representative traces. Right: mean cytosolic [Ca^{2+}] increase. n = 26.

(E) Resting cytosolic [Ca^{2+}]. n = 32.

In (B)–(E), data are presented as mean ± SEM. *p < 0.05, **p < 0.01, ***p < 0.001, t test (two tailed, unpaired).

(F) Immunofluorescence image of a denervated MCU-Flag (MCU)-transfected TA muscle section. Antibodies against Flag tag and dystrophin to mark the sarcolemma were used. Scale bar, 100 μm.

(legend continued on next page)

2010). We then drew on anabolic pathways. PGC-1α4, a novel isoform of the transcriptional regulator of mitochondriogenesis, PGC-1α, was shown to induce muscle hypertrophy, impinging on major anabolic routes, such as the IGF1-Akt/PKB axis (Ruas et al., 2012). *Pgc1-α4* correlated with MCU expression and with a cluster of genes involved in muscle hypertrophy. This was particularly clear in the adult muscle, where other *Pgc1-α* isoforms were not concomitantly modulated. As to the downstream effectors, we could demonstrate MCU-dependent phosphorylation of Akt and its downstream targets, 4E-BP1 and GSK3β. In agreement with these data, a marked increase in protein synthesis was measured in experiments of puromycin incorporation in nascent peptides.

Finally, MCU overexpression significantly counteracts denervation atrophy by markedly increasing the $[Ca^{2+}]_{mt}$ rises evoked by SR Ca^{2+} release and K^+-induced depolarization. The clarification of this novel pathway will thus represent an important task for the future, with potential applications of utmost relevance for the pharmacological targeting of muscle loss in disease states and aging.

EXPERIMENTAL PROCEDURES

Expression Plasmids

MCU-GFP, MCU-Flag, MCU-Cherry, and mtGCaMP6m have been reported previously (De Stefani et al., 2011; Logan et al., 2014; Raffaello et al., 2013). pZac2.1, pZac2.1-LacZ, and pZacf-U6-luc-ZsGreen (shluc-ZsGreen) were purchased from the University of Pennsylvania Vector Core.

For pZac2.1-MCU, MCU-Flag was amplified from MCU expression plasmid (De Stefani et al., 2011) with the primers 5′-CTCGAGGCCACCATGG CGGCCGCCGCAGGTAG-3′ (forward) and 5′-GAATTCTCACTTATCGTCGT CATCCTTGT-3′ (reverse) and cloned into XhoI-EcoRI sites of pZac2.1.

For shMCU-ZsGreen, the MCU targeting sequence was inserted into BamHI-EcoRI sites of shluc-ZsGreen with the primers 5′-GATCGGATCCGA GATGACCGTGAATCTTCAAGAGAGATTCACGGTCATCTCGGATCTTTTTG-3′ (forward) and 5′-AATTCAAAAAGATCCGAGATGACCGTGAATCTCTCTTGAA GATTCACGGTCATCTCGGATCC-3′ (reverse).

For shMCU-Cherry and shluc-Cherry, ZsGreen cassettes of shMCU-ZsGreen and of shluc-ZsGreen were substituted with the mCherry cassette of pmCherry-N1 (Clontech Laboratories) at NheI-NotI sites.

AAV Production

AAV-MCU and AAV-LacZ were produced from pZac2.1-MCU and pZac2.1-LacZ, respectively; AAV-shMCU and AAV-shluc were produced from pZacf-U6-MCU-ZsGreen and pZacf-U6-luc-ZsGreen, respectively. AAV vectors were purchased from Vector BioLabs or prepared by the AAV Vector Unit at ICGEB Trieste (http://www.icgeb.org/avu-core-facility.html), as described previously (Arsic et al., 2004), with few modifications. The titer of recombinant AAVs was determined by quantifying vector genomes (vg) packaged into viral particles by real-time PCR against a standard curve of a plasmid containing the vector genome (Zentilin et al., 2001); values obtained were in the range of 1×10^{12} to 1×10^{13} vg/ml.

In Vivo AAV Infection, DNA Transfection, and Denervation

In vivo experiments were performed in accordance with the Italian law D. L.vo n°26/2014.

AAV Infection

For experiments in the newborn, 10^{10} vg were injected into the hindlimb of 4- to 6-day-old male CD1 mice. Muscles were subsequently analyzed 1 or 2 months post-injection as reported in Results. An average of 64% of fibers were positive for the AAV infections. For experiments in the adult, male CD1 mice were used. EDL muscles were isolated through a small hindlimb incision, and 10^{10} vg were injected along the muscle length. Muscles were analyzed 15 days post-injection. An average of 72% of fibers were positive for the AAV infections.

DNA Transfection and Denervation

The TA and FDB muscles of adult male CD1 mice were transfected as previously reported (DiFranco et al., 2009; Sandri et al., 2004). Denervation was achieved by cutting the sciatic nerve high in the thigh.

Microarray Data

Raw data are available in the GEO database (accession number GSE60931). Detailed microarray methods are described in Supplemental Experimental Procedures.

ACCESSION NUMBERS

The GEO accession number for the microarray data reported in this paper is GSE60931.

SUPPLEMENTAL INFORMATION

Supplemental Information includes Supplemental Experimental Procedures, five figures, and three tables and can be found with this article online at http://dx.doi.org/10.1016/j.celrep.2015.01.056.

AUTHOR CONTRIBUTIONS

R.R. and C.M. conceived the project and wrote the manuscript. C.M., G.G., I.Z., A.R., A.B., S.Z., G.P., and D.D.S. performed in vivo and ex vivo experiments. S.B. performed EM experiments and analyses and wrote relative text. F.C. and S.C. performed microarray experiments and analyses and wrote relative text. L.Z. prepared AAVs and assisted with AAV experiments. M.S. co-supervised experiments on hypertrophy pathways. D.D.S. co-supervised Ca^{2+} measurements. F.P. supervised EM experiments and wrote relative text. G.L. supervised microarray experiments.

ACKNOWLEDGMENTS

The authors are grateful to Stefano Schiaffino, Alessandra Zulian, and Denis Vecellio Reane for helpful discussion. This research was supported by grants from the European Union (ERC mitoCalcium, no. 294777 to R.R.); Italian Telethon Foundation (GPP10005A to R.R.; GGP13213 to F.P.); Italian Ministries of Health (Ricerca Finalizzata to R.R.); Italian Ministries of Education, University and Research (PRIN to R.R., FIRB to R.R., FIRB Futuro in Ricerca RBFR10EGVP_002 to C.M., and FIRB Futuro in Ricerca RBFR13A20K 2013 to S.B.); University of Padova (Progetto di Ateneo to C.M.); NIH (grant 1P01AG025532-01A1 to R.R.; subcontract of RO1 AR059646 to F.P.); Cariparo and Cariplo Foundations (to R.R.); and the Italian Association for Cancer Research (AIRC) (to R.R.).

Received: September 5, 2014
Revised: December 23, 2014
Accepted: January 24, 2015
Published: February 26, 2015

(G) Fiber-size analysis of TA muscles upon denervation and MCU-Flag (MCU) overexpression (>800 fibers per muscle; n = 4).
(H and I) AAV-MCU protects from atrophy in the adult when injected in the newborn. (H) Hindlimb muscles of newborn mice were injected with AAV-MCU. Two months later, the sciatic nerve was cut. TA muscle fiber size was analyzed 3, 7, and 14 days after denervation. (I) Fiber-size analysis of AAV-MCU-infected TA muscles upon denervation (> 200 fibers per muscle; n = 3).
In (G) and (I), data are presented as mean ± SEM. *$p < 0.05$, **$p < 0.01$, t test (two tailed, paired). See also Figure S5.

REFERENCES

Alam, M.R., Groschner, L.N., Parichatikanond, W., Kuo, L., Bondarenko, A.I., Rost, R., Waldeck-Weiermair, M., Malli, R., and Graier, W.F. (2012). Mitochondrial Ca2+ uptake 1 (MICU1) and mitochondrial ca2+ uniporter (MCU) contribute to metabolism-secretion coupling in clonal pancreatic β-cells. J. Biol. Chem. *287*, 34445–34454.

Arsic, N., Zacchigna, S., Zentilin, L., Ramirez-Correa, G., Pattarini, L., Salvi, A., Sinagra, G., and Giacca, M. (2004). Vascular endothelial growth factor stimulates skeletal muscle regeneration in vivo. Mol. Ther. *10*, 844–854.

Baughman, J.M., Perocchi, F., Girgis, H.S., Plovanich, M., Belcher-Timme, C.A., Sancak, Y., Bao, X.R., Strittmatter, L., Goldberger, O., Bogorad, R.L., et al. (2011). Integrative genomics identifies MCU as an essential component of the mitochondrial calcium uniporter. Nature *476*, 341–345.

Boncompagni, S., Rossi, A.E., Micaroni, M., Beznoussenko, G.V., Polishchuk, R.S., Dirksen, R.T., and Protasi, F. (2009). Mitochondria are linked to calcium stores in striated muscle by developmentally regulated tethering structures. Mol. Biol. Cell *20*, 1058–1067.

Brini, M., De Giorgi, F., Murgia, M., Marsault, R., Massimino, M.L., Cantini, M., Rizzuto, R., and Pozzan, T. (1997). Subcellular analysis of Ca2+ homeostasis in primary cultures of skeletal muscle myotubes. Mol. Biol. Cell *8*, 129–143.

Cárdenas, C., Miller, R.A., Smith, I., Bui, T., Molgó, J., Müller, M., Vais, H., Cheung, K.H., Yang, J., Parker, I., et al. (2010). Essential regulation of cell bioenergetics by constitutive InsP3 receptor Ca2+ transfer to mitochondria. Cell *142*, 270–283.

De Stefani, D., and Rizzuto, R. (2014). Molecular control of mitochondrial calcium uptake. Biochem. Biophys. Res. Commun. *449*, 373–376.

De Stefani, D., Raffaello, A., Teardo, E., Szabò, I., and Rizzuto, R. (2011). A forty-kilodalton protein of the inner membrane is the mitochondrial calcium uniporter. Nature *476*, 336–340.

DiFranco, M., Quinonez, M., Capote, J., and Vergara, J. (2009). DNA transfection of mammalian skeletal muscles using in vivo electroporation. J. Vis. Exp. *32*, 1520.

Drago, I., De Stefani, D., Rizzuto, R., and Pozzan, T. (2012). Mitochondrial Ca2+ uptake contributes to buffering cytoplasmic Ca2+ peaks in cardiomyocytes. Proc. Natl. Acad. Sci. USA *109*, 12986–12991.

Goodman, C.A., Mabrey, D.M., Frey, J.W., Miu, M.H., Schmidt, E.K., Pierre, P., and Hornberger, T.A. (2011). Novel insights into the regulation of skeletal muscle protein synthesis as revealed by a new nonradioactive in vivo technique. FASEB J. *25*, 1028–1039.

Herrero, J., Valencia, A., and Dopazo, J. (2001). A hierarchical unsupervised growing neural network for clustering gene expression patterns. Bioinformatics *17*, 126–136.

Joiner, M.L., Koval, O.M., Li, J., He, B.J., Allamargot, C., Gao, Z., Luczak, E.D., Hall, D.D., Fink, B.D., Chen, B., et al. (2012). CaMKII determines mitochondrial stress responses in heart. Nature *491*, 269–273.

Logan, C.V., Szabadkai, G., Sharpe, J.A., Parry, D.A., Torelli, S., Childs, A.M., Kriek, M., Phadke, R., Johnson, C.A., Roberts, N.Y., et al.; UK10K Consortium (2014). Loss-of-function mutations in MICU1 cause a brain and muscle disorder linked to primary alterations in mitochondrial calcium signaling. Nat. Genet. *46*, 188–193.

Mammucari, C., Schiaffino, S., and Sandri, M. (2008). Downstream of Akt: FoxO3 and mTOR in the regulation of autophagy in skeletal muscle. Autophagy *4*, 524–526.

Marchi, S., Lupini, L., Patergnani, S., Rimessi, A., Missiroli, S., Bonora, M., Bononi, A., Corrà, F., Giorgi, C., De Marchi, E., et al. (2013). Downregulation of the mitochondrial calcium uniporter by cancer-related miR-25. Curr. Biol. *23*, 58–63.

Murphy, E., Pan, X., Nguyen, T., Liu, J., Holmström, K.M., and Finkel, T. (2014). Unresolved questions from the analysis of mice lacking MCU expression. Biochem. Biophys. Res. Commun. *449*, 384–385.

Pan, X., Liu, J., Nguyen, T., Liu, C., Sun, J., Teng, Y., Fergusson, M.M., Rovira, I.I., Allen, M., Springer, D.A., et al. (2013). The physiological role of mitochondrial calcium revealed by mice lacking the mitochondrial calcium uniporter. Nat. Cell Biol. *15*, 1464–1472.

Qiu, J., Tan, Y.W., Hagenston, A.M., Martel, M.A., Kneisel, N., Skehel, P.A., Wyllie, D.J., Bading, H., and Hardingham, G.E. (2013). Mitochondrial calcium uniporter Mcu controls excitotoxicity and is transcriptionally repressed by neuroprotective nuclear calcium signals. Nat. Commun. *4*, 2034.

Raffaello, A., De Stefani, D., Sabbadin, D., Teardo, E., Merli, G., Picard, A., Checchetto, V., Moro, S., Szabò, I., and Rizzuto, R. (2013). The mitochondrial calcium uniporter is a multimer that can include a dominant-negative pore-forming subunit. EMBO J. *32*, 2362–2376.

Rizzuto, R., De Stefani, D., Raffaello, A., and Mammucari, C. (2012). Mitochondria as sensors and regulators of calcium signalling. Nat. Rev. Mol. Cell Biol. *13*, 566–578.

Ruas, J.L., White, J.P., Rao, R.R., Kleiner, S., Brannan, K.T., Harrison, B.C., Greene, N.P., Wu, J., Estall, J.L., Irving, B.A., et al. (2012). A PGC-1α isoform induced by resistance training regulates skeletal muscle hypertrophy. Cell *151*, 1319–1331.

Rudolf, R., Mongillo, M., Magalhães, P.J., and Pozzan, T. (2004). In vivo monitoring of Ca(2+) uptake into mitochondria of mouse skeletal muscle during contraction. J. Cell Biol. *166*, 527–536.

Sandri, M., Sandri, C., Gilbert, A., Skurk, C., Calabria, E., Picard, A., Walsh, K., Schiaffino, S., Lecker, S.H., and Goldberg, A.L. (2004). Foxo transcription factors induce the atrophy-related ubiquitin ligase atrogin-1 and cause skeletal muscle atrophy. Cell *117*, 399–412.

Schiaffino, S., and Mammucari, C. (2011). Regulation of skeletal muscle growth by the IGF1-Akt/PKB pathway: insights from genetic models. Skelet. Muscle *1*, 4.

Tarasov, A.I., Semplici, F., Ravier, M.A., Bellomo, E.A., Pullen, T.J., Gilon, P., Sekler, I., Rizzuto, R., and Rutter, G.A. (2012). The mitochondrial Ca2+ uniporter MCU is essential for glucose-induced ATP increases in pancreatic β-cells. PLoS ONE *7*, e39722.

Zentilin, L., Marcello, A., and Giacca, M. (2001). Involvement of cellular double-stranded DNA break binding proteins in processing of the recombinant adeno-associated virus genome. J. Virol. *75*, 12279–12287.